iScience

CellPress

Article

Novel Bacterial Diversity and Fragmented eDNA Identified in Hyperbiofilm-Forming *Pseudomonas aeruginosa* Rugose Small Colony Variant

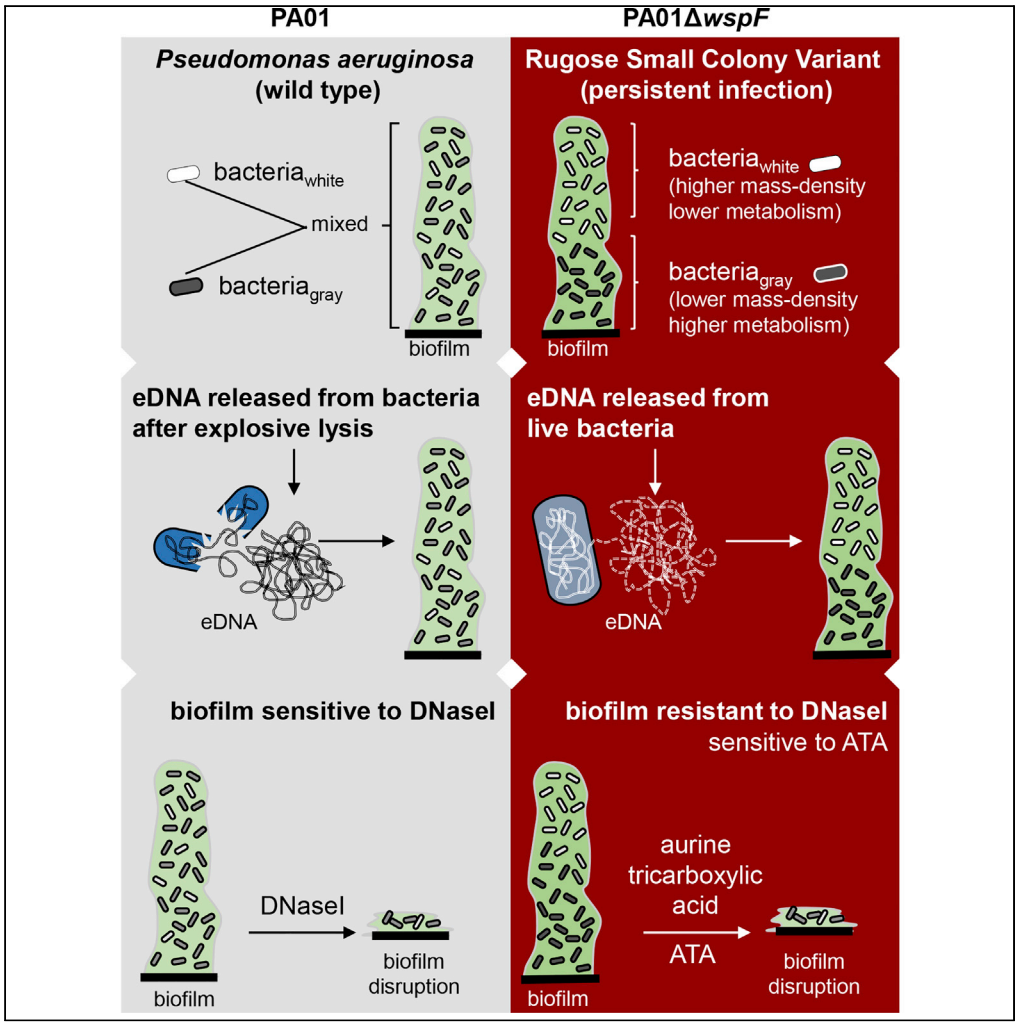

Binbin Deng, Subhadip Ghatak, Subendu Sarkar, ..., Daniel J. Wozniak, David W. McComb, Chandan K. Sen

cksen@iu.edu

HIGHLIGHTS

Hyperbiofilm clinical isolate PAO1Δ*wspF* contain unique cell state and organization

Bacterial cells in PAO1Δ*wspF* biofilm are morphologically and physiologically unique

PAO1Δ*wspF*, unlike PAO1 that undergo explosive lysis, release eDNA from live cells

Aurine tricarboxylic acid, not DNaseI as for PAO1, disrupts PAO1Δ*wspF* biofilm

Deng et al., iScience *23*, 100827
February 21, 2020
https://doi.org/10.1016/j.isci.2020.100827

iScience

CellPress

Article

Novel Bacterial Diversity and Fragmented eDNA Identified in Hyperbiofilm-Forming *Pseudomonas aeruginosa* Rugose Small Colony Variant

Binbin Deng,[2,3,6] Subhadip Ghatak,[1,6] Subendu Sarkar,[1,6] Kanhaiya Singh,[1] Piya Das Ghatak,[1] Shomita S. Mathew-Steiner,[1] Sashwati Roy,[1] Savita Khanna,[1] Daniel J. Wozniak,[4] David W. McComb,[3,5] and Chandan K. Sen[1,2,7,*]

SUMMARY

***Pseudomonas aeruginosa* biofilms represent a major threat to health care. Rugose small colony variants (RSCV) of *P. aeruginosa*, isolated from chronic infections, display hyperbiofilm phenotype. RSCV biofilms are highly resistant to antibiotics and host defenses. This work shows that RSCV biofilm aggregates consist of two distinct bacterial subpopulations that are uniquely organized displaying contrasting physiological characteristics. Compared with that of PAO1, the extracellular polymeric substance of RSCV PAO1Δ*wspF* biofilms presented unique ultrastructural characteristics. Unlike PAO1, PAO1Δ*wspF* released fragmented extracellular DNA (eDNA) from live cells. Fragmented eDNA, thus released, was responsible for resistance of PAO1Δ*wspF* biofilm to disruption by DNaseI. When added to PAO1, such fragmented eDNA enhanced biofilm formation. Disruption of PAO1Δ*wspF* biofilm was achieved by aurine tricarboxylic acid, an inhibitor of DNA-protein interaction. This work provides critical novel insights into the contrasting structural and functional characteristics of a hyperbiofilm-forming clinical bacterial variant relative to its own wild-type strain.**

INTRODUCTION

Biofilms are highly resistant to antibiotics and host immune defenses because of their structural and phenotypic characteristics (Høiby et al., 2010; Borlee et al., 2010). Extracellular polymeric substance (EPS) plays pivotal roles in the structural organization of biofilms (Flemming et al., 2016; Gunn et al., 2016). In addition to reinforcing the physical strength of biofilm (Borlee et al., 2010), EPSs also promote microbial interaction and communication (Flemming and Wingender, 2010; Flemming, 2016), enhance horizontal gene transfer (Savage et al., 2013; Merod and Wuertz, 2014), trap nutrients, and even provide nutrients to the persistent bacteria during starvation (Mulcahy et al., 2010). The clinical rugose small colony variant (RSCV) of *Pseudomonas aeruginosa* is hyperactive in biofilm formation during chronic infection (Pestrak et al., 2018; Hauser et al., 2011; Wei et al., 2011). Under laboratory conditions, emergence of some RSCVs relies on loss-of-function mutations in the methylesterase-encoding gene *wspF* (Pu et al., 2018). Such mutations in RSCV result in constitutive overexpression of both Pel and Psl exopolysaccharides (Jennings et al., 2015). RSCVs are difficult to eradicate and are responsible for recurrent or chronic infections (Neut et al., 2007). In biofilms, RSCVs are deeply embedded in self-produced hydrated EPSs (Costerton et al., 1999). The Psl and Pel exopolysaccharides, together with extracellular DNA (eDNA), serve as structural components of the biofilm matrix (Jennings et al., 2015).

The structural characteristics of bacterial biofilm contribute to their pathogenicity (O'Connell et al., 2006). Diversity in the structural elements of bacterial biofilm has been of interest (Donlan, 2002). Insight into biofilm ultrastructure is likely to unveil novel therapeutic strategies for eradicating persistent infection. In this work we sought to investigate the ultrastructure of the hyperbiofilm-producing *P. aeruginosa* RSCV strain PAO1Δ*wspF* with reference to its isogenic strain PAO1. Both strains are of direct clinical relevance (Goltermann and Tolker-Nielsen, 2017).

P. aeruginosa RSCVs cause persistent infection, because they are recalcitrant to antibiotics and host immune cells (Proctor et al., 2006; Evans, 2015; Pestrak et al., 2018; Wozniak and Parsek, 2014). Scanning transmission electron microscopy (STEM) tomography is powerful in unveiling the structural characteristics with nanometer-scale spatial resolution (Aoyama et al., 2009; Sousa and Leapman, 2012). Insight gained from

[1]Department of Surgery, Indiana Center for Regenerative Medicine and Engineering, Indiana University School of Medicine, Indianapolis, IN 46202, USA

[2]Department of Surgery, The Ohio State University Wexner Medical Center, Columbus, OH 43210, USA

[3]Center for Electron Microscopy and Analysis, College of Engineering, The Ohio State University, Columbus, OH 43212, USA

[4]Departments of Microbial Infection and Immunity, Microbiology, Infectious Disease Institute, Ohio State University, Columbus, OH 43210, USA

[5]Department of Materials Science and Engineering, The Ohio State University, Columbus, OH 43210, USA

[6]These authors contributed equally

[7]Lead Contact

*Correspondence: cksen@iu.edu

https://doi.org/10.1016/j.isci.2020.100827

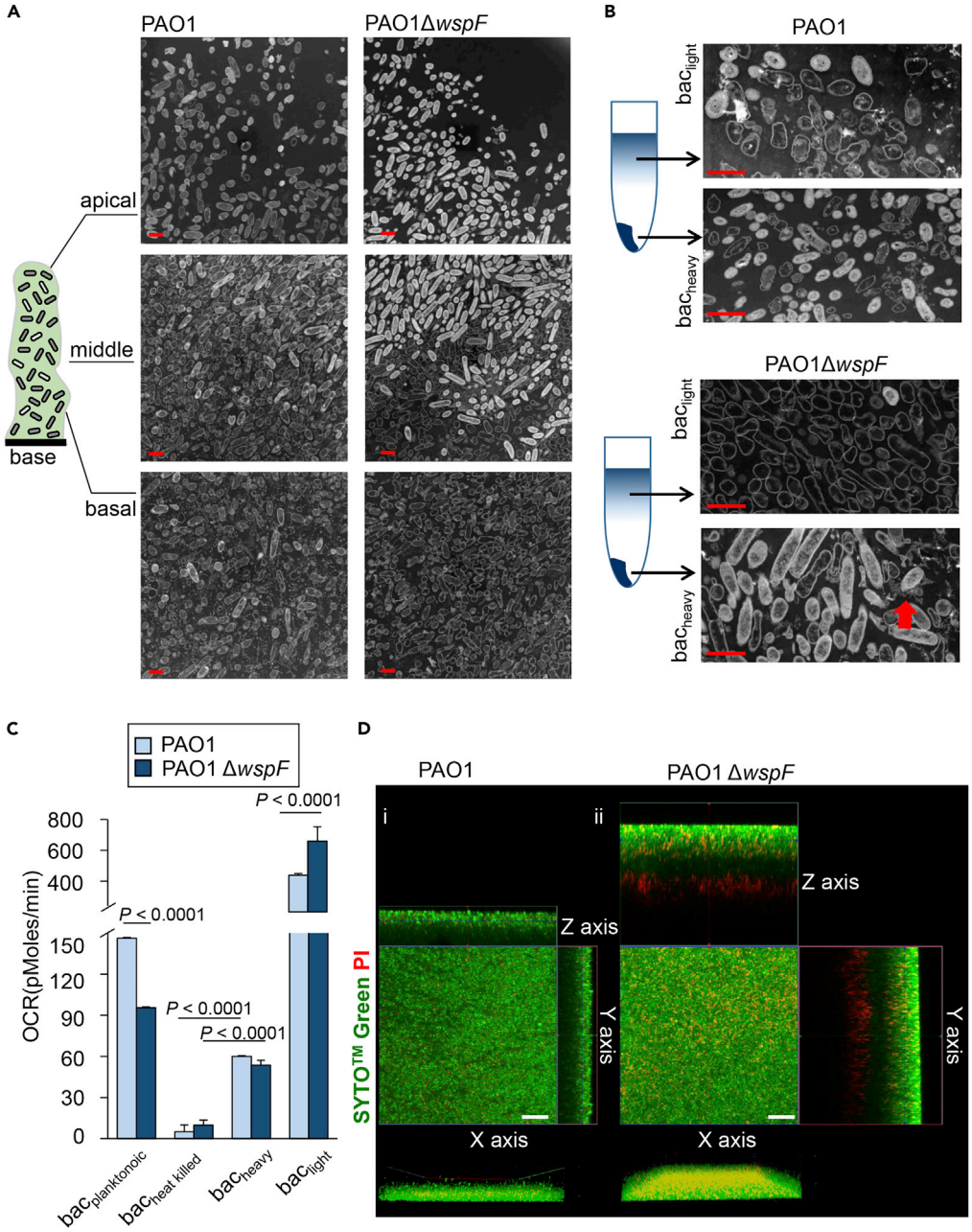

Figure 1. STEM Imaging and Tomography Revealed Distinct Bacterial Phenotype Distribution in PAO1 and PAO1ΔwspF Biofilms

(A) STEM images of the *in vitro* PAO1 biofilm and PAO1Δ*wspF* biofilm showed a distinct spatial distribution of two bacterial phenotypes named as $bacteria_{white}$ and $bacteria_{gray}$. Unlike that in PAO1 biofilm where the $bacteria_{white}$ and $bacteria_{gray}$ were homogenously distributed throughout the biofilm, $bacteria_{white}$ and $bacteria_{gray}$ are segregated in the PAO1Δ*wspF* biofilm. $Bacteria_{white}$ was observed from lower-middle to apical area, and $bacteria_{gray}$ was observed from basal to lower-middle area. The pseudo-colored rendering derived from 3D STEM tomographic structure of the PAO1 biofilm and PAO1Δ*wspF* biofilm. Scale bar, 1 μm.

(B) STEM images showed the successful separation of $bacteria_{white}$ and $bacteria_{gray}$ in PAO1 biofilm and PAO1Δ*wspF* biofilm. The bac_{light} fraction and bac_{heavy} fraction were obtained from the density gradient centrifugation of biofilm following DNaseI treatment. Scale bar, 1 μm.

Figure 1. *Continued*

(C) Real-time changes in oxygen consumption rate (OCR, in picomoles of molecular oxygen per minute) measured on a Seahorse XFe Extracellular Flux Analyzer in bac_{light} fraction and bac_{heavy} fraction of PAO1 and PAO1Δ*wspF* biofilm. (n = 10). Data are mean ± SD.

(D) Live dead staining of PAO1 and PAO1Δ*wspF* biofilm using SYTO Green and PI at 48 h. Scale bar, 20 μm.

See also Figures S1 and S2.

STEM imaging and tomography has led to novel mechanistic hypothesis. It was thus gleaned that inhibition of EPS protein-eDNA interaction is a specifically effective strategy to dismantling biofilms formed by RSCVs.

RESULTS

Distinct Bacterial Phenotype Distribution in PAO1 and PAO1Δ*wspF* Biofilm

This work provides insights into the 3D-reconstructed ultrastructure of bacterial biofilm using STEM tomography. STEM imaging and tomography offer the opportunity to investigate the ultrastructure of aggregated macromolecular complexes in the EPS with nanometer-scale spatial resolution. In STEM, a focused electron beam (<1 nm diameter) scans across the specimen and the transmitted signal is collected pixel by pixel. Images collected as a function of sample rotation angle (with respect to the electron beam direction) enable 3D reconstruction (Aoyama et al., 2009; Sousa and Leapman, 2012). In STEM images of non-crystalline materials recorded using a high-angle angular dark field (HAADF) detector, such as the biofilm specimens (Figures 1A and 1B), mass thickness is the dominant contrast mechanism. A region that has higher mass density or is thicker will scatter more electrons. Consequently, the HAADF-STEM signal will be more intense, and the region will exhibit "white" contrast. Unlike conventional confocal microscopy (Figure S1A), STEM imaging of PAO1 and PAO1Δ*wspF* biofilms revealed two distinct subpopulations that were uniquely organized in the hyperbiofilm strain (PAO1Δ*wspF*) compared with that in the wild-type (PAO1) variety (Figures 1A and S1B, Video S1). Two distinct subpopulations, "white" and "grey" contrast, were noted in the STEM-HAADF images (Figure 1A). Henceforth, in this report, these subpopulations are referred to as $bacteria_{white}$ and $bacteria_{gray}$, respectively. In the PAO1 biofilm, $bacteria_{white}$ and $bacteria_{gray}$ were homogenously distributed throughout the biofilm (Figure 1A). In contrast, the PAO1Δ*wspF* biofilm showed a segregated spatial distribution such that $bacteria_{white}$ were found at the apical and $bacteria_{gray}$ at the basal regions of the biofilm (Figure 1A). Thus, $bacteria_{white}$ were localized toward the air interface, whereas $bacteria_{gray}$ were more proximal to the nutrient-supplying basal interface. As the microtomed specimens have negligible variations in thickness, the effect of thickness on the scale of contrast variations can be discounted. Thus the differences between $bacteria_{white}$ and $bacteria_{gray}$ are attributed to their mass-density difference. On the basis of these observations, a density gradient centrifugation approach was developed to separate the two different subpopulations of bacteria: $bacteria_{white}$ and $bacteria_{gray}$ (Figure S2). The pellet obtained after density gradient centrifugation was designated as bac_{heavy} and the supernatant as bac_{light} (Figures 1B and S2). STEM-HAADF images showed that the bac_{heavy} fraction (Figure 1B) was predominantly comprised of $bacteria_{white}$. The bac_{light} fraction was predominantly $bacteria_{gray}$ (Figure 1B). PAO1Δ*wspF* biofilm bacteria were in strict adherence to these rules validating our notion that the $bacteria_{white}$ have higher mass density than the $bacteria_{gray}$. The separation of $bacteria_{white}$ and $bacteria_{gray}$ from PAO1 biofilm cells after density gradient centrifugation was not as efficient as that in the PAO1Δ*wspF* biofilm cells. Although the predominance of $bacteria_{white}$ was indeed more in the bac_{heavy} fraction of PAO1 biofilm, some were present in the bac_{light} fraction as well (Figure 1B).

In our effort to investigate functional contrasts between bac_{light} and the bac_{heavy}, cellular respiration was studied using a real-time prokaryotic respiration assay (SeaHorse XFe extracellular flux analyzer) (Lobritz et al., 2015). Compared with bac_{heavy}, bac_{light} showed elevated oxygen consumption indicative of higher aerobic metabolism of biofilm bacteria localized toward the nutrient interface. Respiration of bac_{heavy} was detected, compared with heat-killed bacteria, indicating that bac_{heavy} were metabolically less active, but not dead (Figure 1C).

In another experimental system studying intact biofilm, the DNA-intercalating dye propidium iodide (PI) stained abundantly toward the air interface in PAO1Δ*wspF* biofilms (Figure 1D). Taken together, PI stain as well as cellular respiration leads to the conclusion that $bacteria_{white}$ have reduced metabolic capacity but have much higher abundance of eDNA in their EPS microenvironment. Thus, this work draws a direct connection between the structural elements and functional properties of bacterial subpopulations within the same biofilm. Importantly, in the

hyperbiofilm RSCV, the basal subpopulation proximal to the nutrient interface was metabolically hyperactive compared with the same subpopulation in the wild-type strain (Figure 1C). Such observation may be explained by the finding that in PAO1, the basal hypermetabolic bacteria$_{gray}$ population is somewhat diluted by the presence of few hypometabolic bacteria$_{white}$ cells. However, in PAO1Δ*wspF* biofilm, the basal subpopulation consists of a homogeneous population of hypermetabolic bacteria$_{gray}$ cells.

PAO1Δ*wspF* Release Segmented eDNA in Biofilm

In PAO1, lysis of a subpopulation of bacteria contributes to the eDNA pool, which in turn facilitates the self-organization of biofilm structures (Whitchurch et al., 2002; Turnbull et al., 2016). In our experimental system investigating PAO1, consistent findings were noted. Lysed PAO1 indeed contributed to eDNA as observed from live cell imaging with cell-impermeant DNA-binding dye TOTO-1 that specifically stains eDNA (Figure 2A, Video S2). STEM imaging revealed the products of bacterial lysis within the PAO1 biofilm (Figure 2B top left). In PAO1Δ*wspF* biofilm, however, remnants of lysed bacteria were rarely evident (Figure 2B bottom left). Further investigation into the source of eDNA in EPS of PAO1Δ*wspF* revealed extrusion of DNA from live cells into the extracellular compartment (Figure 2A and Video S3). Such process was not associated with bacterial lysis as reported for PAO1 (Figure 2A). Because PI stains both eDNA and intracellular DNA of bacteria with compromised wall integrity, the PI data from PAO1Δ*wspF* biofilm alone is inadequate to draw any conclusion. To address this, live cell imaging with TOTO-1 and PI was performed in PAO1Δ*wspF* (Figure 2C). Unlike heat-killed PAO1Δ*wspF*, evidence of PI^{-} bacteria showing TOTO-1 staining supports the fact that PAO1Δ*wspF* possess a distinct mechanism of extruding DNA without undergoing lysis as commonly seen in PAO1 (Figure 2C, Videos S4 and S5).

HAADF-STEM imaging and tomography provides unprecedented insight into the ultrastructure of a wild-type and its corresponding hyperbiofilm variant. In PAO1, heterogeneous mixture of globular debris was abundant in EPS (Figures 2B and S3A, Video S6). In contrast, EPS of PAO1Δ*wspF* biofilm showed thread-like structures associated with vesicular structures (Figures 2B bottom right, S3A right, Video S6). The observed heterogeneous mixture of globular debris in PAO1, which appears white in HAADF-STEM images, was sensitive to DNaseI treatment supporting the notion that it is eDNA (Figure S3C). In PAO1, DNaseI treatment completely eliminated all globular debris-like structures and compromised the structural integrity of the biofilm to a point where fixation of samples for HAADF-STEM imaging was challenging (Figure S3B). In the few cases wherein samples could be processed, distorted morphology of individual PAO1 bacteria were observed (Figure S3C). In cases wherein the structural integrity of the PAO1 biofilm was completely lost, the sloughed off samples were pelleted by centrifugation. Such pellets were processed for STEM imaging as described. Of note, the resulting images provided information on the content of each sample and not on its structure (Figure S3D). Elimination of the globular debris-like structures following DNaseI treatment was evident (Figure S3E). This observation further supports the conclusion that the heterogeneous mixture of globular debris was eDNA. However, unlike the PAO1 biofilm, the PAO1Δ*wspF* biofilm was resistant to DNaseI treatment (Figure S3B). Following DNaseI treatment, PAO1Δ*wspF* biofilm retained appreciable structural integrity including some DNaseI-resistant structures in the EPS (Figure S3C). These retained structures associated with aggregates of vesicular structures only in the EPS of PAO1Δ*wspF* (area pointed by red arrow in Figures S3C, S3F, and S3G). Thus, there are clear differences in the structural characteristics of the biofilm of the wild-type and its variant.

eDNA in PAO1Δ*wspF* Biofilm Represented Only Part of PAO1Δ*wspF* Genome DNA

Explosive lysis of *P. aeruginosa* contributes eDNA to EPS of PAO1 (Turnbull et al., 2016). Thus, whole-genomic DNA was expected in the EPS of a PAO1 biofilm (Allesen-Holm et al., 2006). Interestingly, abundance of eDNA in the biofilm of PAO1 and PAO1Δ*wspF* was comparable (Figures 3A and 3B). Our findings on PAO1, the wild-type reference strain of this study, showed that indeed the eDNA of PAO1 biofilm was intact and represented the entire genome (Figures 2D and 3C–3E). Compared with PAO1 biofilm, eDNA of PAO1Δ*wspF* biofilm was mostly fragmented (Figures 2D and 3E) with size range of 25–400 bp (Figure S4). In the context of evidence on DNA extrusion from live PAO1Δ*wspF* bacteria and lack of entire genome representation in the eDNA (Figures 3C–3E) it is concluded that these hyperbiofilm bacteria are capable of contributing eDNA to the extracellular compartment without necessarily having to go through the suicidal path of explosive lysis. In this process, abundant eDNA is deposited as needed for biofilm structure. In the context of hyperbiofilm PAO1Δ*wspF* bacteria, an important question that arises is whether the eDNA is fragmented within the cell and then exported or whether intact DNA exported by the live cell undergoes fragmentation in the extracellular space. In the current work, next-generation sequencing of eDNA from

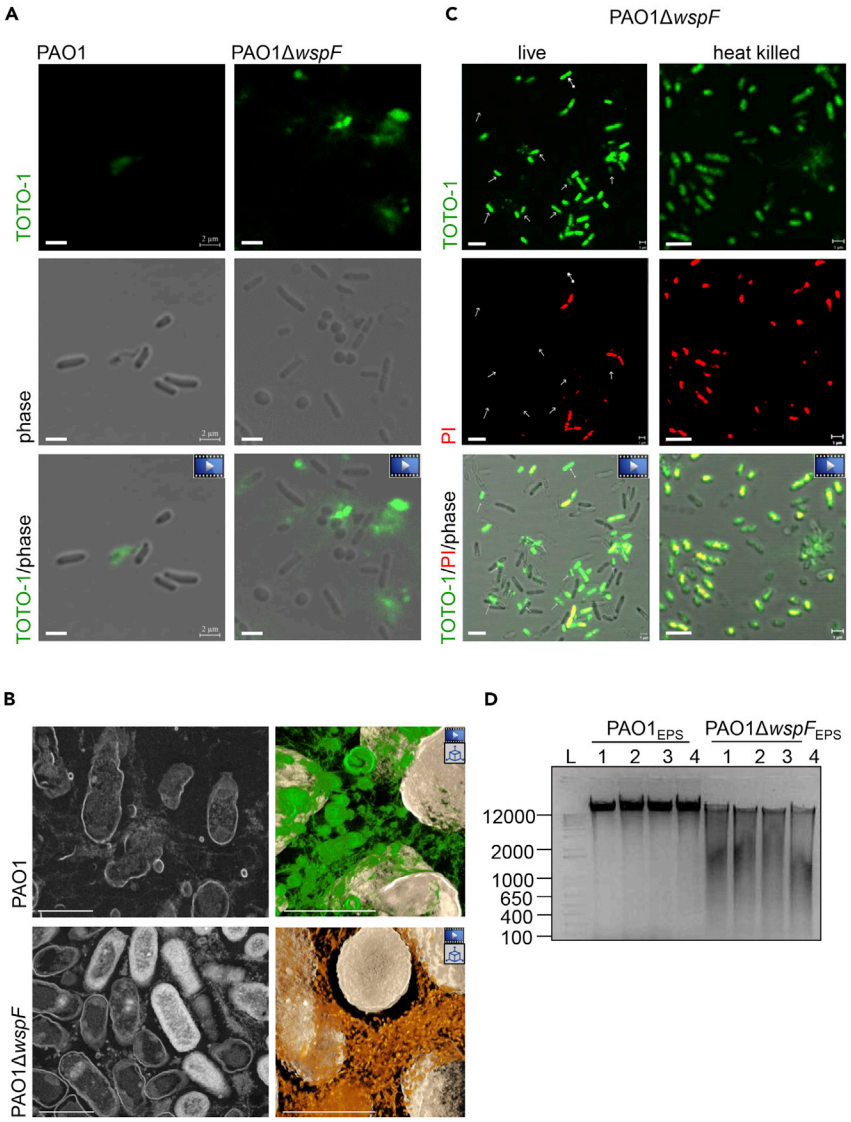

Figure 2. PAO1Δ*wspF* Release Segmented eDNA in Biofilm

(A) Confocal microscopic images showing release of eDNA in PAO1 after lysis (left), whereas the PAO1Δ*wspF* showed release of eDNA in intact bacteria (right). Scale bar, 2 μm Indicate movies in the supplement (Videos S2 and S3).

(B) Representative STEM image (top left) showing lysis of PAO1 from 12 different areas of biofilm rich in such fragmented bacteria from middle to basal regions of PAO1 biofilm. 2D rendering of 3D structures (right) of the PAO1 biofilm and PAO1Δ*wspF* biofilm. Cell lysis and release of eDNA (top left) in PAO1 biofilm was observed. Evidence of cell lysis and release of eDNA in PAO1Δ*wspF* biofilm was relatively limited (bottom left). Green and golden pseudo-colors were added in the right images to highlight EPS in PAO1 and PAO1Δ*wspF*, respectively. Movies are available for images with film frame icon (Video S6). Scale bar, 500 nm. Indicates movies in the supplement. Indicates 3D reconstruction of the STEM images.

(C) Confocal microscopic images showing release of eDNA by live PAO1Δ*wspF*. Scale bar, 2 μm. Indicates movies in the supplement (Videos S4 and S5).

(D) Agarose gel electrophoresis of the DNA isolated from the EPS showed that eDNA is mainly intact in PAO1 biofilm; however, in PAO1Δ*wspF*, eDNA is fragmented.

See also Figure S3.

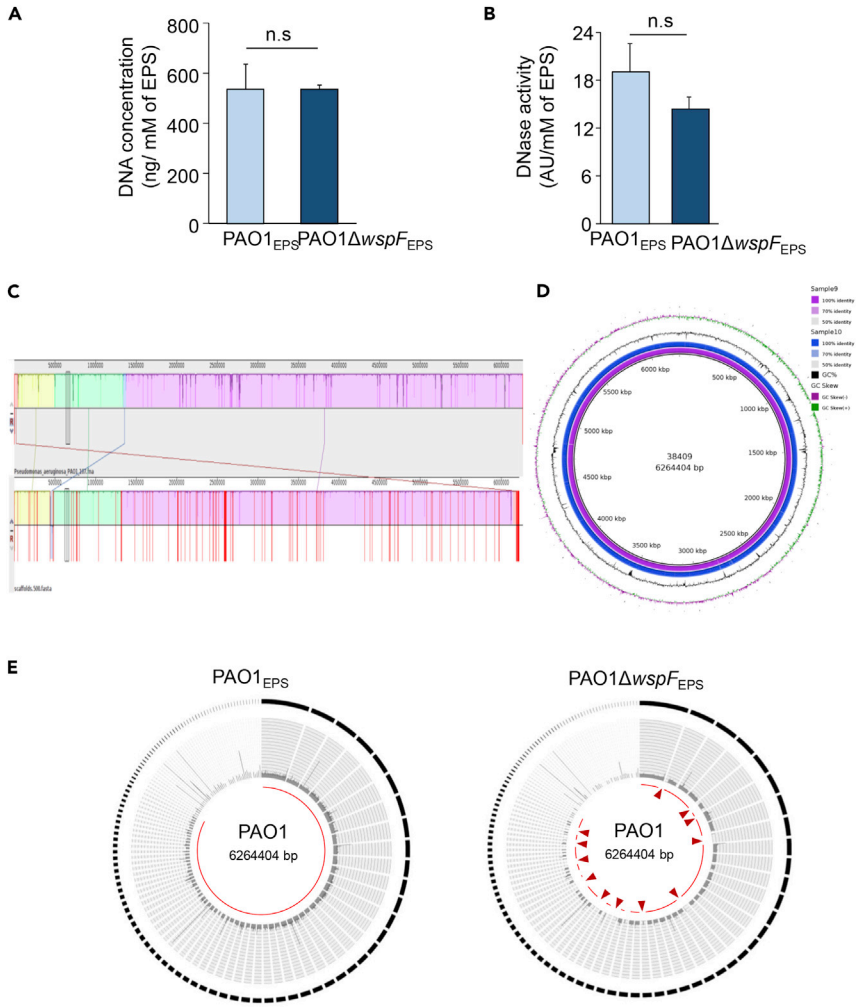

Figure 3. eDNA in PAO1Δ*wspF* Biofilm Was Found to Consist of Only Part of PAO1Δ*wspF* Genome DNA

(A and B) Quantification of (A) eDNA and (B) DNase activity from the EPS of PAO1 and PAO1ΔwspF showed no significant difference in the eDNA content and DNase activity. (n = 4) Data are mean ± SD

(C) Sorted alignment with PAO1 reference sequence.

(D) Circular genome map of PAO1 (accession number: NC_002516) showing the genomic islands (GIs) predicted by IslandViewer and prophages. From the outside: circle 1, GC skew; circle 2, GC content; circle 3, PAO1ΔwspF genome (sample 10); circle 4, PAO1 genome (sample 9). The scale in kilobase pair (kbp) is indicated at the innermost region of the map.

(E) Comparison of assembled contigs of PAO1 genomic DNA and PAO1ΔwspF genomic DNA compared with PAO1 reference genome. See also Figure S4.

the PAO1 biofilm was identical to that from the PAO1 genome (Figure 3E), supporting the previously reported observation of explosive lysis of PAO1 (Turnbull et al., 2016). PAO1Δ*wspF* biofilm did not follow that pattern. In this case, the eDNA showed little resemblance to the PAO1 genome (Figure 3E). This observation becomes even more interesting considering the fact that both total eDNA content and DNase activity were comparable in the EPS of PAO1 and PAO1Δ*wspF* biofilms (Figures 3A and 3B). These observations led us to test the hypothesis that unlike PAO1, hyperbiofilm-forming PAO1Δ*wspF* bacteria possess the unique ability to extrude DNA fragments as part of bolstering their biofilm structure.

Interaction of Fragmented DNA with EPS Protein Results in Formation of Robust Biofilm

In the current work, addition of EPS from PAO1Δ*wspF* to PAO1 augmented biofilm formation. However, addition of EPS from PAO1 to PAO1Δ*wspF* did not influence its biofilm-forming ability (Figures S5A and

S5B). To elucidate the functional significance of EPS component eDNA in biofilm formation, intact genomic DNA was isolated from PAO1 and subjected to DNaseI digestion (Figure S5C). Addition of this fragmented DNA to PAO1 showed no significant change in bacterial growth curve when compared with addition of intact DNA to PAO1 (Figure S5D). However, such addition of fragmented DNA accelerated biofilm formation in PAO1. Compared to addition of intact DNA, fragmented DNA showed clear enhancement of biofilm formation (Figures 4A and S5E). Most biofilm matrix proteins stain positive with SYPRO Ruby (Ahire et al., 2016). Compared to intact DNA, fragmented eDNA was more effective in interacting with biofilm matrix proteins (Figures 4B and S5F). Consistently, crystal violet assay for biofilm quantification supported the same conclusion demonstrating that fragmented DNA enhanced biofilm formation (Figure 4C). DNA is known to possess adhesive property, which facilitates interaction with other biomolecules to ensure structural integrity of the biofilm (Okshevsky and Meyer, 2015). Observations of the current study lend credence to the notion that fragmented eDNA, as opposed to intact DNA, provides additional advantage to the process of biofilm formation. Interestingly, hyperbiofilm bacteria utilize this edge to their advantage.

Bacteria with hyperbiofilm characteristics employed fragmented eDNA to achieve better interaction with macromolecules in the EPS (Figures 4D–4F). To test the significance of such interaction in biofilm formation, the EPS isolated from PAO1Δ*wspF* biofilm was incubated with aurine tricarboxylic acid (ATA), a pharmacological inhibitor of protein-nucleic acid binding (Gonzalez et al., 1979). ATA significantly compromised the biofilm-forming ability of PAO1 (Figure S6A). Protein-nucleic acid binding played a significant role in biofilm formation by RSCV (Figures 4D–4F and S6B). However, ATA did not affect bacterial growth as evident from PAO1Δ*wspF* growth curve (Figure S6C). Specifically, ATA limited protein-nucleic acid interaction in PAO1Δ*wspF* biofilm (Figures 4F and S6D).

DISCUSSION

P. aeruginosa RSCVs cause persistent infection, because they are recalcitrant to antibiotics and host immune cells (Proctor et al., 2006; Evans, 2015; Pestrak et al., 2018). Structural characteristics of bacterial biofilm contribute to their pathogenicity (O'Connell et al., 2006). This work is the first to compare the biofilm ultrastructure of a parent strain of *P. aeruginosa* with an isogenic RSCV. While commonly used confocal laser scanning microscopy or SEM techniques to understand biofilm structure are of value (Azeredo et al., 2017; Lawrence and Neu, 1999; Schlafer and Meyer, 2017), they are somewhat limited in resolution. This work reports the first evidence for the presence and distribution of two distinct bacterial populations, apical bacteria$_{white}$ and basal bacteria$_{gray}$, in the PAO1Δ*wspF* biofilm. The distribution of these two distinct bacterial populations in the PAO1Δ*wspF* biofilm was not only morphological but also physiological.

Findings of this work demonstrate that the oxygen consumption of basal bacteria$_{gray}$ was elevated compared with that of the apical bacteria$_{white}$ population. These data were consistent with the previous report from the spatial distribution of *Escherichia coli* macrocolony biofilms (Serra and Hengge 2014). According to that report, bacteria in the basal region were dividing with minimal ribosomal synthesis, whereas bacteria in the apical region displayed limited cell division yet robust ribosomal synthesis (Serra and Hengge 2014). This work reports the first identification and separation of these two distinct bacterial populations.

A growing body of research now acknowledges the presence of extracellular forms of DNA and their role as important structural components of the biofilm matrix (Bockelmann et al., 2006). Previously, eDNA was thought to result largely from the lysis of cells or release of plasmids. However, seminal studies by Whitchurch et al. showed that eDNA is a major component of the *P. aeruginosa* EPS (Whitchurch et al., 2002). Hence, we looked for the composition and origin of eDNA present in the EPS as a variable for biofilm stability in PAO1ΔwspF compared with PAO1. The formation of a biofilm also relies on the structural proteins that provide the three-dimensional architectural integrity and functionality (Hobley et al., 2015). Negatively charged eDNA interacts with positively charged proteins (Dengler et al., 2015) and polysaccharide (Wang et al., 2015; Jennings et al., 2015) to form the structural backbone of the bacterial biofilm. How eDNA stabilizes the *P. aeruginosa* biofilm structure and contributes to antimicrobial tolerance remains unclear. This work recognizes the fact that intact bacterial DNA presents itself as eDNA in PAO1 biofilm supporting the contention that such DNA is delivered by bacterial cell lysis. Explosive lysis of *P. aeruginosa* has been shown to be responsible for eDNA contents of biofilm (Turnbull et al., 2016). eDNA in *P. aeruginosa* is similar to whole-genome DNA (Allesen-Holm et al., 2006). Consistently, our work reports intact eDNA in the PAO1

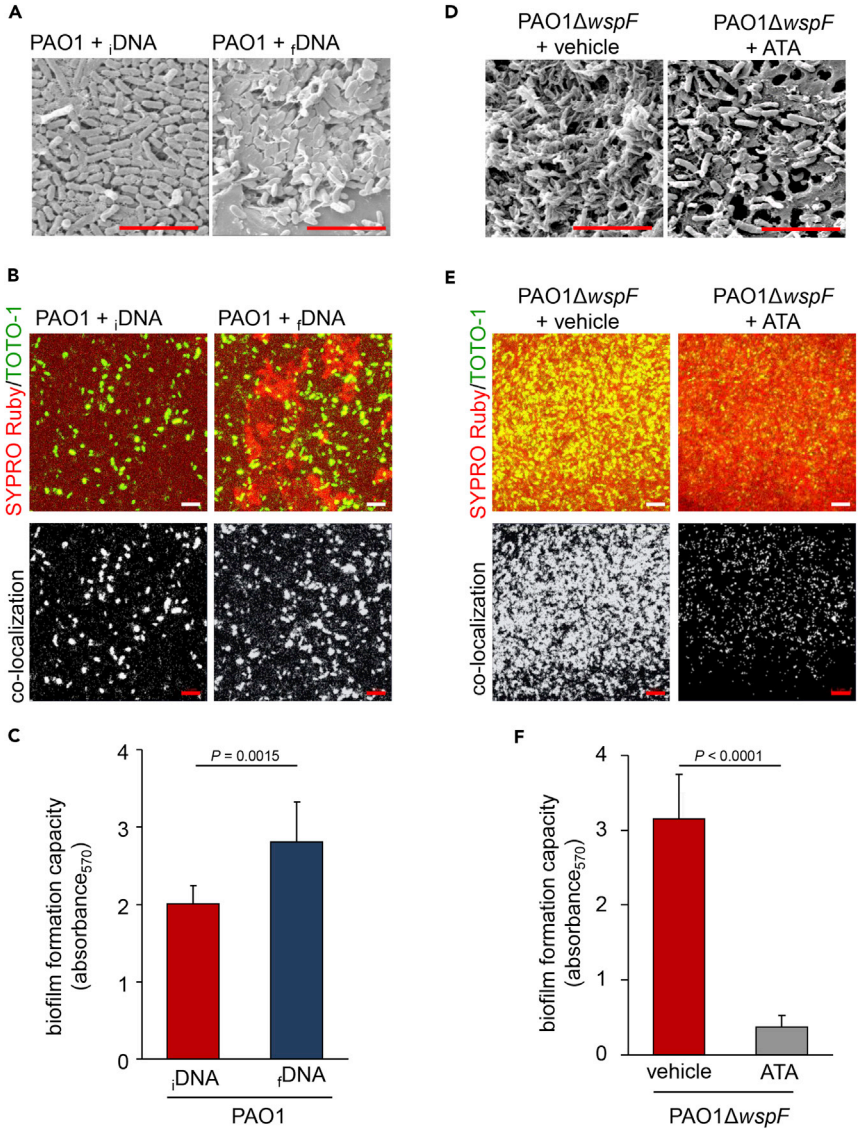

Figure 4. Interaction of Fragmented DNA with EPS Protein Results in Formation of Robust Biofilm

(A) SEM images of PAO1 biofilm at 12 h treated with 500 ng intact genomic DNA ($_i$DNA) and fragmented genomic DNA ($_f$DNA). Scale bar, 5 μm.

(B) Confocal microscopic images showing SYPRO Ruby (red) and TOTO-1 (green) staining of PAO1 biofilm at 12 h treated with 500 ng intact genomic DNA ($_i$DNA) and fragmented genomic DNA ($_f$DNA). The co-localization of EPS protein (red) and eDNA (green) is shown as white dots. Scale bar, 5 μm.

(C) Crystal violet assay of PAO1 biofilm at 12 h treated with 500 ng intact genomic DNA ($_i$DNA), and fragmented genomic DNA ($_f$DNA) (n = 8). Data are mean ± SD.

(D) SEM images of PAO1Δ*wspF* biofilm at 24 h treated with buffer and ATA. Scale bar, 5 μm.

(E) Confocal microscopic images showing SYPRO Ruby (red) and TOTO-1 (green) staining of PAO1Δ*wspF* biofilm at 24 h treated with buffer and ATA. The co-localization of EPS protein (red) and eDNA (green) are shown as white dots. Scale bar, 5 μm.

(F) Crystal violet assay of PAO1Δ*wspF* biofilm at 24 h treated with buffer and ATA (n = 8). Inhibition of DNA-protein interaction compromised *in vitro* PAO1Δ*wspF* biofilm formation. Data are mean ± SD.

See also Figures S5 and S6.

biofilm. Interestingly, in a PAO1Δ*wspF* biofilm, eDNA was mostly fragmented. Thus, whether the DNA is fragmented in the matrix or processed inside the bacteria emerges as an interesting question. That bacterial cellular DNA may be exported by live cells has been recently shown in *Staphylococcus aureus* (DeFrancesco et al., 2017). Genome-wide screening for genes involved in forming robust *S. aureus* biofilms

identified gdpP and xdrA that are involved in the release of eDNA (DeFrancesco et al., 2017). Whether, unlike PAO1, viable non-lytic PAO1Δ*wspF* is capable of digesting part of its own DNA and extruding such digest to support the biofilm structure needs further investigation.

Consistent with the notion that eDNA provides critical support to the biofilm structure, DNaseI treatment compromised PAO1 biofilm. In contrast, the structural integrity of PAO1Δ*wspF* biofilm was mostly unaffected by such enzymatic treatment. After DNaseI treatment, although eDNA was removed at the basal region, thread-like eDNA persisted from the middle to the apical region of the PAO1Δ*wspF* biofilm. Emerging studies reveal that interaction between eDNA and other EPS components may stabilize biofilm structure (Schwartz et al., 2016; Hu et al., 2012; Jennings et al., 2015; Das et al., 2013b). For example, pyocyanin, a metabolite of *P. aeruginosa*, interacts with eDNA enhancing bacteria cell aggregation (Das et al., 2013a). In *P. aeruginosa* biofilm, negatively charged eDNA and positively charged Pel polysaccharide are cross-linked by ionic forces (Jennings et al., 2015). The Psl-eDNA fiber-like structure helps to form the biofilm skeleton in *P. aeruginosa* (Wang et al., 2015).

Biofilms are more susceptible to antibiotics after eDNA is removed by DNase (Kaplan et al., 2012; Tetz et al., 2009). Although DNaseI treatment did not dismantle the biofilm structure of PAO1Δ*wspF*, it was helpful in separating bac_{light} and bac_{heavy} cells, pointing toward a potential role of eDNA in the adhesion of these cells. In *P. aeruginosa*, addition of eDNA enhances biofilm structure (Yang et al., 2009). On the other hand, addition of excessive eDNA may inhibit planktonic bacteria growth and biofilm formation (Mulcahy et al., 2008). In this work, cell growth of *P. aeruginosa* was not altered in the presence of digested DNA at a concentration of 100 ng/mL (Figure S5D). Interestingly, addition of genomic DNA digest increased DNA-protein interaction and accelerated biofilm formation. Indeed, nucleoid-associated proteins are known to connect eDNA strands in *Haemophilus influenzae* biofilm (Goodman et al., 2011). Targeting eDNA-protein interactions disperses *Burkholderia cenocepacia* biofilms (Novotny et al., 2013). Proteomic findings of this work revealed the co-existence of higher abundance of nucleic acid-binding protein and fragmented eDNA at the apical $bacteria_{white}$ region. Inhibition of DNA-protein interaction with ATA blunted biofilm formation by PAO1Δ*wspF*.

STEM images reported herein provide unprecedented comparative insight into the structure of prototypical *P. aeruginosa* and its isogenic RSCV strain PAO1Δ*wspF*. This work reports the first evidence for the presence and segregated distribution of two distinct bacterial populations, apical $bacteria_{white}$ and basal $bacteria_{gray}$, in the PAO1Δ*wspF* biofilm. These bacteria were not only phenotypically different but also showed difference in oxygen consumption rate. Furthermore, resistance to DNase digestion in RSCV was attributed to the fact that the eDNA in the EPS was fragmented. The strategy to inhibit protein-DNA interaction using ATA was effective in dismantling biofilms formed by RSCV. Taken together, this work provides unprecedented visual cues into the structure of biofilm formed by *P. aeruginosa* upholding clear structural as well as functional differences between wild-type and its hyperbiofilm variant.

Limitations of the Study

Study of the PAO1Δ*wspF* led to the observation of two different bacterial subpopulations displaying distinct spatial organization in biofilm aggregates. Previous studies have reported explosive lysis of wild-type *P. aeruginosa* that contributes eDNA to EPS (Turnbull et al., 2016). We have reproduced that observation in PAO1. However, such explosive lysis was not observed predominantly in the PAO1Δ*wspF*. Live cell imaging and NGS data support that hyperbiofilm-forming PAO1Δ*wspF* bacteria possess the unique ability to extrude DNA fragments from living bacteria as part of bolstering its biofilm structure. These novel observations are based on the study of a single strain that was selected because it is a clinical isolate and therefore of relevance to human health care. Although in our observation we have not noted explosive lysis of PAO1Δ*wspF* bacteria, the possibility that different *P. aeruginosa* in other habitats may undergo explosive lysis remains open. We acknowledge that our data may be specific to this clinical isolate and that different *P. aeruginosa* may behave differently. Results of this work introduce a new paradigm wherein specific details such as aggregate size and organization may vary across different strains.

METHODS

All methods can be found in the accompanying Transparent Methods supplemental file (Videos S7 and S8).

SUPPLEMENTAL INFORMATION

Supplemental Information can be found online at https://doi.org/10.1016/j.isci.2020.100827.

ACKNOWLEDGMENTS

We sincerely thank Prof. Mervin C. Yoder for his critical appraisal of the manuscript. We thank Dr. Puneet Khandelwal and Dr. Dolly Khona for their help with super-resolution laser scanning confocal microscopy. This work was supported by the US National Institutes of Health grants NR015676 to C.K.S.

AUTHOR CONTRIBUTIONS

Conceptualization, C.K.S.; Methodology, C.K.S., S.G., and B.D.; Investigation and Validation, B.D., S.G., S.S., K.S., P.D.G., and S.M.-S., Formal Analysis, B.D., S.G, S.S., K.S., S.M.-S., S.R., and S.K.; Writing – Original Draft, B.D., S.G., S.S., K.S., S.M.-S., S.K., S.R, D.W.M., D.J.W., and C.K.S.; Visualization, B.D., S.G., and C.K.S; Funding Acquisition, C.K.S.; Resources, C.K.S., D.J.W., and D.W.M.; Supervision, C.K.S., S.K., S.R., D.W.M., and D.J.W.

DECLARATION OF INTERESTS

The authors declare no competing interests.

Received: June 30, 2019
Revised: November 30, 2019
Accepted: January 6, 2020
Published: February 21, 2020

REFERENCES

Ahire, J.J., Hattingh, M., Neveling, D.P., and Dicks, L.M. (2016). Copper-containing anti-biofilm nanofiber scaffolds as a wound dressing material. PLoS One *11*, e0152755.

Allesen-Holm, M., Barken, K.B., Yang, L., Klausen, M., Webb, J.S., Kjelleberg, S., Molin, S., Givskov, M., and Tolker-Nielsen, T. (2006). A characterization of DNA release in Pseudomonas aeruginosa cultures and biofilms. Mol. Microbiol. *59*, 1114–1128.

Aoyama, K., Takagi, T., Hirase, A., and Miyazawa, A. (2009). STEM tomography for thick biological specimens. Ultramicroscopy *109*, 70.

Azeredo, J., Azevedo, N.F., Briandet, R., Cerca, N., Coenye, T., Costa, A.R., Desvaux, M., Di Bonaventura, G., Hébraud, M., Jaglic, Z., et al. (2017). Critical review on biofilm methods. Crit. Rev. Microbiol. *43*, 313–351.

Bockelmann, U., Janke, A., Kuhn, R., Neu, T.R., Wecke, J., Lawrence, J.R., and Szewzyk, U. (2006). Bacterial extracellular DNA forming a defined network-like structure. FEMS Microbiol. Lett. *262*, 31–38.

Borlee, B.R., Goldman, A.D., Murakami, K., Samudrala, R., Wozniak, D.J., and Parsek, M.R. (2010). Pseudomonas aeruginosa uses a cyclic-di-GMP-regulated adhesin to reinforce the biofilm extracellular matrix. Mol. Microbiol. *75*, 827–842.

Costerton, J.W., Stewart, P.S., and Greenberg, E.P. (1999). Bacterial biofilms: a common cause of persistent infections. Science *284*, 1318–1322.

Das, T., Kutty, S.K., Kumar, N., and Manefield, M. (2013a). Pyocyanin facilitates extracellular DNA binding to Pseudomonas aeruginosa influencing cell surface properties and aggregation. PLoS One *8*, e58299.

Das, T., Sehar, S., and Manefield, M. (2013b). The roles of extracellular DNA in the structural integrity of extracellular polymeric substance and bacterial biofilm development. Environ. Microbiol. Rep. *5*, 778–786.

DeFrancesco, A.S., Masloboeva, N., Syed, A.K., DeLoughery, A., Bradshaw, N., Li, G.W., Gilmore, M.S., Walker, S., and Losick, R. (2017). Genome-wide screen for genes involved in eDNA release during biofilm formation by Staphylococcus aureus. Proc. Natl. Acad. Sci. U S A *114*, E5969–E5978.

Dengler, V., Foulston, L., DeFrancesco, A.S., and Losick, R. (2015). An electrostatic net model for the role of extracellular DNA in biofilm formation by Staphylococcus aureus. J. Bacteriol. *197*, 3779–3787.

Donlan, R.M. (2002). Biofilms: microbial life on surfaces. Emerg. Infect. Dis. *8*, 881–890.

Evans, T.J. (2015). Small colony variants of Pseudomonas aeruginosa in chronic bacterial infection of the lung in cystic fibrosis. Future Microbiol. *10*, 231–239.

Flemming, H.C. (2016). EPS—then and now. Microorganisms *4*, 41.

Flemming, H.C., and Wingender, J. (2010). The biofilm matrix. Nat. Rev. Microbiol. *8*, 623–633.

Flemming, H.C., Wingender, J., Szewzyk, U., Steinberg, P., Rice, S.A., and Kjelleberg, S. (2016). Biofilms: an emergent form of bacterial life. Nat. Rev. Microbiol. *14*, 563–575.

Goltermann, L., and Tolker-Nielsen, T. (2017). Importance of the exopolysaccharide matrix in antimicrobial tolerance of Pseudomonas aeruginosa aggregates. Antimicrob. Agents Chemother. *61*, e02696–e02716.

Gonzalez, R.G., Blackburn, B.J., and Schleich, T. (1979). Fractionation and structural elucidation of the active components of aurintricarboxylic acid, a potent inhibitor of protein nucleic acid interactions. Biochim. Biophys. Acta *562*, 534–545.

Goodman, S.D., Obergfell, K.P., Jurcisek, J.A., Novotny, L.A., Downey, J.S., Ayala, E.A., Tjokro, N., Li, B., Justice, S.S., and Bakaletz, L.O. (2011). Biofilms can be dispersed by focusing the immune system on a common family of bacterial nucleoid-associated proteins. Mucosal Immunol. *4*, 625–637.

Gunn, J.S., Bakaletz, L.O., and Wozniak, D.J. (2016). Whats on the outside matters: the role of the extracellular polymeric substance of gram-negative biofilms in evading host immunity and as a target for therapeutic intervention. J. Biol. Chem. *291*, 12538–12546.

Hauser, A.R., Jain, M., Bar-Meir, M., and McColley, S.A. (2011). Clinical significance of microbial infection and adaptation in cystic fibrosis. Clin. Microbiol. Rev. *24*, 29–70.

Hobley, L., Harkins, C., MacPhee, C.E., and Stanley-Wall, N.R. (2015). Giving structure to the biofilm matrix: an overview of individual strategies and emerging common themes. FEMS Microbiol. Rev. *39*, 649–669.

Høiby, N., Bjarnsholt, T., Givskov, M., Molin, S., and Ciofu, O. (2010). Antibiotic resistance of

bacterial biofilms. Int. J. Antimicrob. Agents *35*, 322–332.

Hu, W., Li, L., Sharma, S., Wang, J., McHardy, I., Lux, R., Yang, Z., He, X., Gimzewski, J.K., Li, Y., and Shi, W. (2012). DNA builds and strengthens the extracellular matrix in myxococcus xanthus biofilms by interacting with exopolysaccharides. PLoS One *7*, e51905.

Jennings, L.K., Storek, K.M., Ledvina, H.E., Coulon, C., Marmont, L.S., Sadovskaya, I., Secor, P.R., Tseng, B.S., Scian, M., Filloux, A., et al. (2015). Pel is a cationic exopolysaccharide that cross-links extracellular DNA in the Pseudomonas aeruginosa biofilm matrix. Proc. Natl. Acad. Sci. U S A *112*, 11353–11358.

Kaplan, J.B., LoVetri, K., Cardona, S.T., Madhyastha, S., Sadovskaya, I., Jabbouri, S., and Izano, E.A. (2012). Recombinant human DNase I decreases biofilm and increases antimicrobial susceptibility in staphylococci. J. Antibiot. *65*, 73–77.

Lawrence, J.R., and Neu, T.R. (1999). Confocal laser scanning microscopy for analysis of microbial biofilms. Methods Enzymol. *310*, 131–144.

Lobritz, M.A., Belenky, P., Porter, C.B., Gutierrez, A., Yang, J.H., Schwarz, E.G., Dwyer, D.J., Khalil, A.S., and Collins, J.J. (2015). Antibiotic efficacy is linked to bacterial cellular respiration. Proc. Natl. Acad. Sci. U S A *112*, 8173–8180.

Merod, R.T., and Wuertz, S. (2014). Extracellular polymeric substance architecture influences natural genetic transformation of Acinetobacter baylyi in biofilms. Appl. Environ. Microbiol. *80*, 7752–7757.

Mulcahy, H., Charron-Mazenod, L., and Lewenza, S. (2008). Extracellular DNA chelates cations and induces antibiotic resistance in Pseudomonas aeruginosa biofilms. PLoS Pathog. *4*, e1000213.

Mulcahy, H., Charron-Mazenod, L., and Lewenza, S. (2010). Pseudomonas aeruginosa produces an extracellular deoxyribonuclease that is required for utilization of DNA as a nutrient source. Environ. Microbiol. *12*, 1621–1629.

Neut, D., van der Mei, H.C., Bulstra, S.K., and Busscher, H.J. (2007). The role of small-colony variants in failure to diagnose and treat biofilm infections in orthopedics. Acta Orthop. *78*, 299–308.

Novotny, L.A., Amer, A.O., Brockson, M.E., Goodman, S.D., and Bakaletz, L.O. (2013). Structural stability of Burkholderia cenocepacia biofilms is reliant on eDNA structure and presence of a bacterial nucleic acid binding protein. PLoS One *8*, e67629.

O'Connell, H.A., Kottkamp, G.S., Eppelbaum, J.L., Stubblefield, B.A., Gilbert, S.E., and Gilbert, E.S. (2006). Influences of biofilm structure and antibiotic resistance mechanisms on indirect pathogenicity in a model polymicrobial biofilm. Appl. Environ. Microbiol. *72*, 5013–5019.

Okshevsky, M., and Meyer, R.L. (2015). The role of extracellular DNA in the establishment, maintenance and perpetuation of bacterial biofilms. Crit. Rev. Microbiol. *41*, 341–352.

Pestrak, M.J., Chaney, S.B., Eggleston, H.C., Dellos-Nolan, S., Dixit, S., Mathew-Steiner, S.S., Roy, S., Parsek, M.R., Sen, C.K., and Wozniak, D.J. (2018). Pseudomonas aeruginosa rugose small-colony variants evade host clearance, are hyper-inflammatory, and persist in multiple host environments. PLoS Pathog. *14*, e1006842.

Proctor, R.A., von Eiff, C., Kahl, B.C., Becker, K., McNamara, P., Herrmann, M., and Peters, G. (2006). Small colony variants: a pathogenic form of bacteria that facilitates persistent and recurrent infections. Nat. Rev. Microbiol. *4*, 295–305.

Pu, M., Sheng, L., Song, S., Gong, T., and Wood, T.K. (2018). Serine hydroxymethyltransferase ShrA (PA2444) controls rugose small-colony variant formation in Pseudomonas aeruginosa. Front. Microbiol. *9*, 315.

Savage, V.J., Chopra, I., and ONeill, A.J. (2013). Staphylococcus aureus biofilms promote horizontal transfer of antibiotic resistance. Antimicrob. Agents Chemother. *57*, 1968–1970.

Schlafer, S., and Meyer, R.L. (2017). Confocal microscopy imaging of the biofilm matrix. J. Microbiol. Methods *138*, 50–59.

Schwartz, K., Ganesan, M., Payne, D.E., Solomon, M.J., and Boles, B.R. (2016). Extracellular DNA facilitates the formation of functional amyloids in Staphylococcus aureus biofilms. Mol. Microbiol. *99*, 123–134.

Serra, D.O., and Hengge, R. (2014). Stress responses go three dimensional – the spatial order of physiological differentiation in bacterial macrocolony biofilms. Environ. Microbiol. *16*, 1455–1471.

Sousa, A.A., and Leapman, R.D. (2012). Development and application of STEM for the biological sciences. Ultramicroscopy *123*, 38–49.

Tetz, G.V., Artemenko, N.K., and Tetz, V.V. (2009). Effect of DNase and antibiotics on biofilm characteristics. Antimicrob. Agents Chemother. *53*, 1204–1209.

Turnbull, L., Toyofuku, M., Hynen, A.L., Kurosawa, M., Pessi, G., Petty, N.K., Osvath, S.R., Cárcamo-Oyarce, G., Gloag, E.S., Shimoni, R., et al. (2016). Explosive cell lysis as a mechanism for the biogenesis of bacterial membrane vesicles and biofilms. Nat. Commun. *7*, 11220.

Wang, S., Liu, X., Liu, H., Zhang, L., Guo, Y., Yu, S., Wozniak, D.J., and Ma, L.Z. (2015). The exopolysaccharide Psl-eDNA interaction enables the formation of a biofilm skeleton in Pseudomonas aeruginosa. Environ. Microbiol. Rep. *7*, 330–340.

Wei, Q., Tarighi, S., Dötsch, A., Häussler, S., Müsken, M., Wright, V.J., Cámara, M., Williams, P., Haenen, S., Boerjan, B., et al. (2011). Phenotypic and genome-wide analysis of an antibiotic-resistant small colony variant (SCV) of Pseudomonas aeruginosa. PLoS One *6*, e29276.

Whitchurch, C.B., Tolker-Nielsen, T., Ragas, P.C., and Mattick, J.S. (2002). Extracellular DNA required for bacterial biofilm formation. Science *295*, 1487.

Wozniak, D.J., and Parsek, M.R. (2014). Surface-associated microbes continue to surprise us in their sophisticated strategies for assembling biofilm communities. F1000prime Rep. *6*, 26.

Yang, L., Nilsson, M., Gjermansen, M., Givskov, M., and Tolker-Nielsen, T. (2009). Pyoverdine and PQS mediated subpopulation interactions involved in Pseudomonas aeruginosa biofilm formation. Mol. Microbiol. *74*, 1380–1392.

iScience, Volume *23*

Supplemental Information

Novel Bacterial Diversity and Fragmented eDNA Identified in Hyperbiofilm-Forming *Pseudomonas aeruginosa* Rugose Small Colony Variant

Binbin Deng, Subhadip Ghatak, Subendu Sarkar, Kanhaiya Singh, Piya Das Ghatak, Shomita S. Mathew-Steiner, Sashwati Roy, Savita Khanna, Daniel J. Wozniak, David W. McComb, and Chandan K. Sen

Figure S1

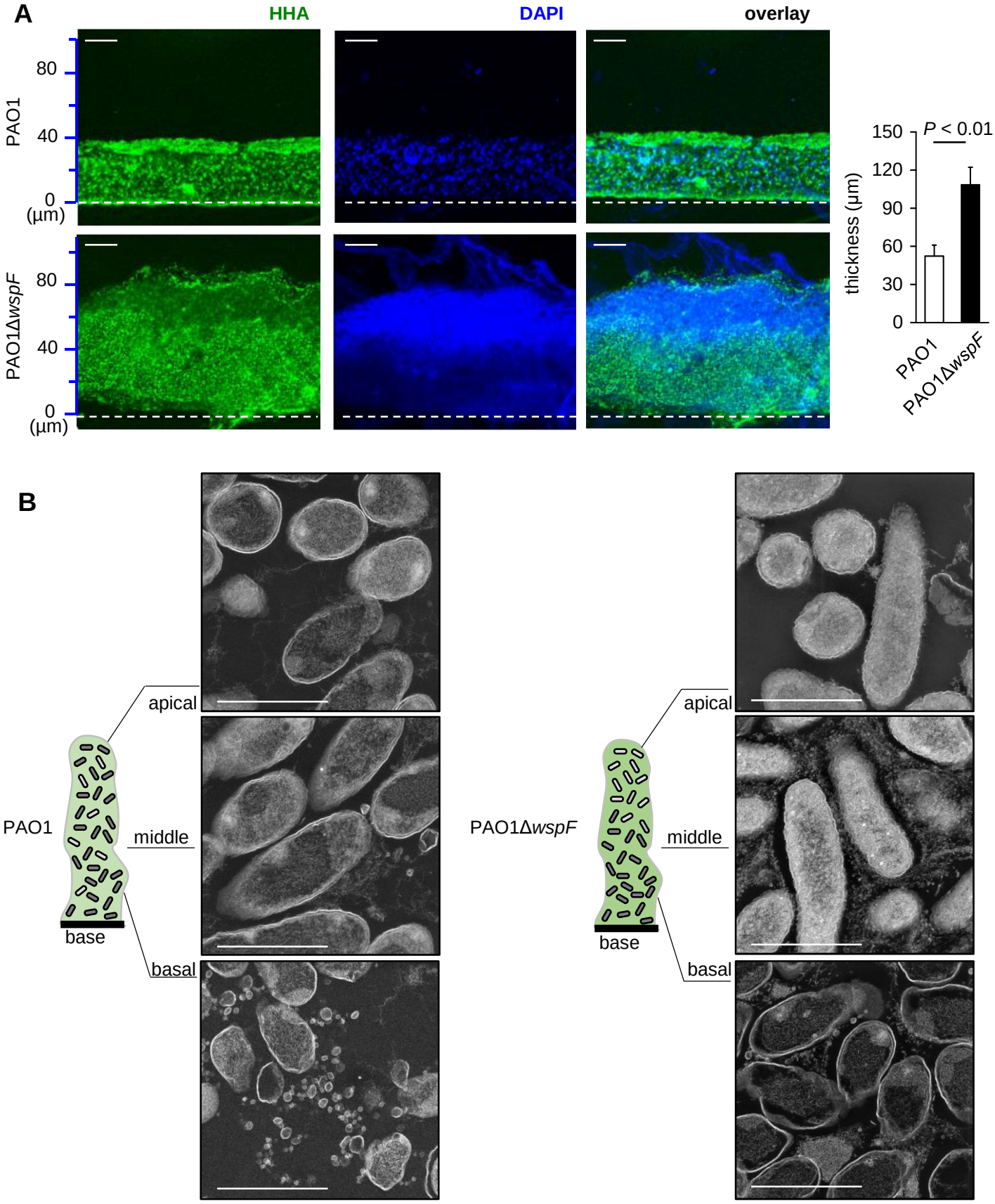

Figure S1. Bacterial segregation in PAO1Δ*wspF* biofilm. Related to Figure 1A. (A) Confocal microscopic images showing the longitudinal section of PAO1 and PAO1Δ*wspF* biofilm after staining with the FITC-HHA lectins (green) and DAPI (blue). Scale bar, 20μm. The white dashed line indicates the PCM membrane. The average thickness of the biofilms are quantified and expressed graphically as mean ± SD. (n=4). (**B**) STEM images showed the biofilms at basal, middle and apical area. Scale bar, 1μm.

Figure S2

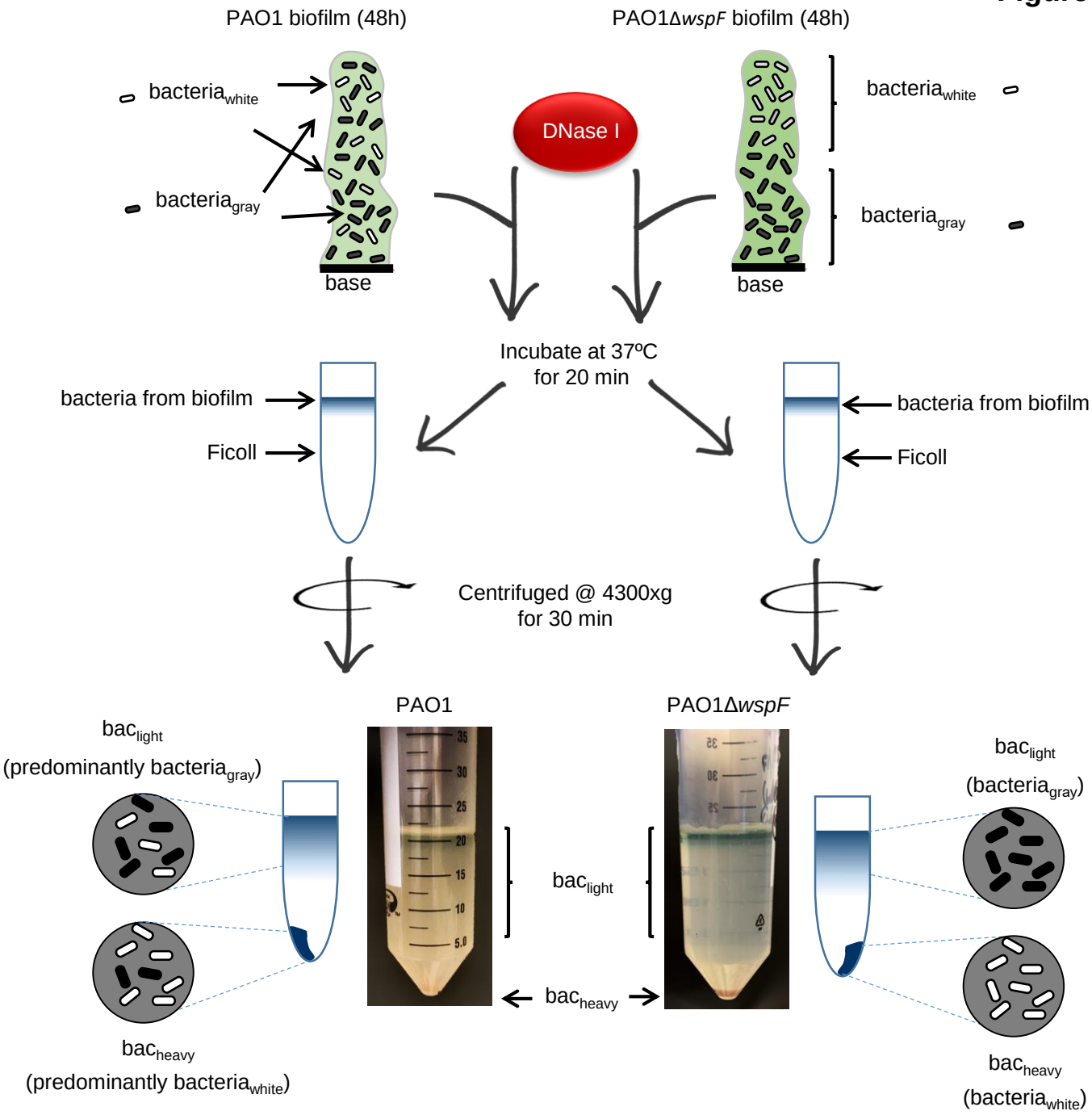

Figure S2. Process of separating bacterial phenotype bacteria$_{white}$ and bacteria$_{gray}$ in PAO1 and PAO1Δ*wspF* biofilm. **Related to Figure 1B.** Schematic diagram showing the process of separating the two different bacterial phenotype from the biofilm using density gradient centrifugation.

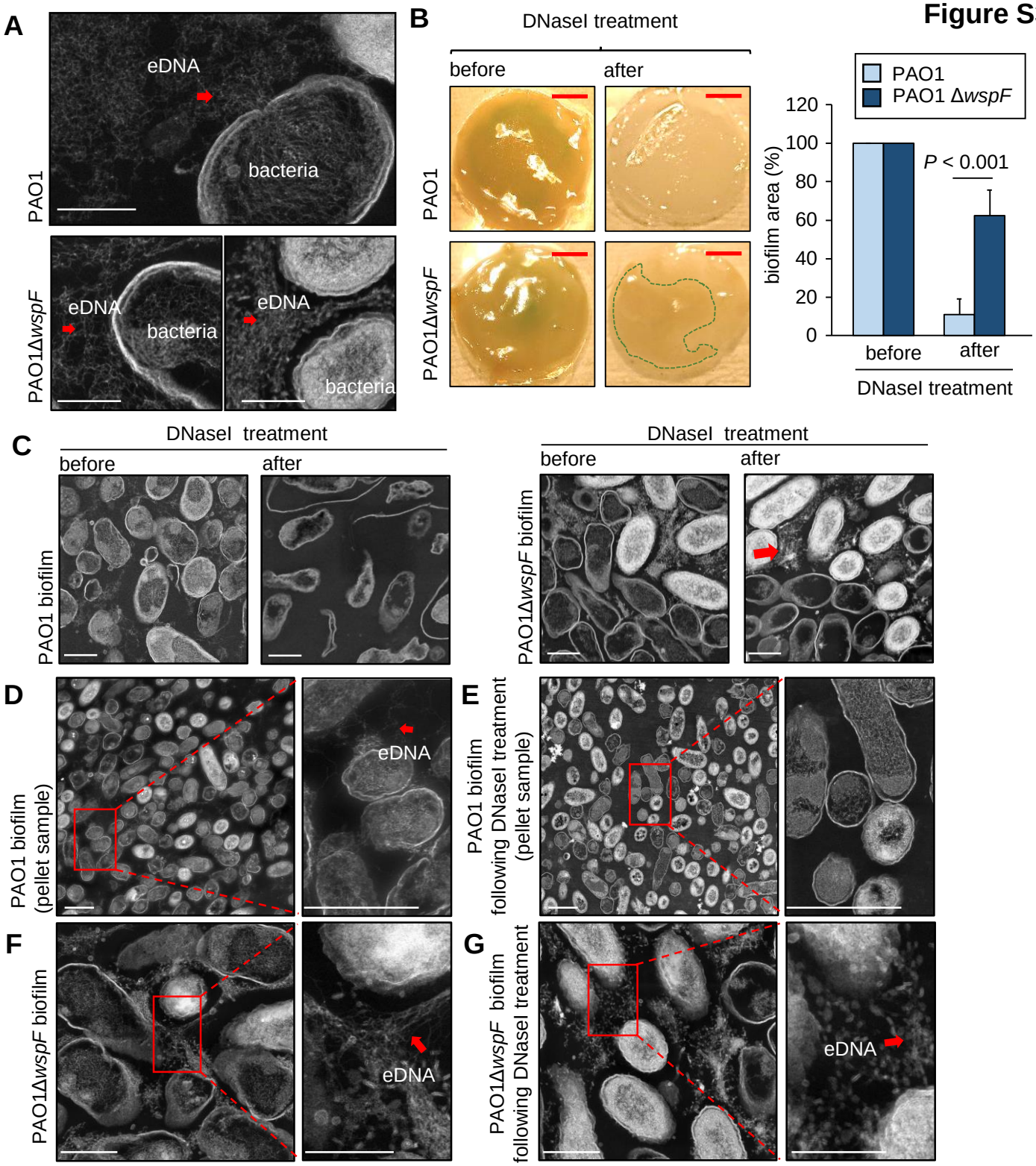

Figure S3. PAO1Δ*wspF* biofilm are resistant to DNaseI digestion. Related to Figure 2. (**A**) eDNA in PAO1 biofilm and PAO1Δ*wspF* biofilm. Upper image showed thread-like eDNA in PAO1 biofilm. Lower left image showed the thread-like eDNA around bacteria$_{gray}$ in PAO1Δ*wspF* biofilm. Lower right image showed the eDNA and cell debris around bacteria$_{white}$ in PAO1Δ*wspF* biofilm. Scale bar, 250nm (**B**) Digital macrophotographs of PAO1 and PAO1Δ*wspF* biofilm before and after DNaseI treatment. The green dotted lines represent the area that remained intact after DNaseI treatment. The area of the biofilm before and after DNaseI treatment were quantified using image J and expressed graphically (n=6). Scale bar, 2.5mm. (**C**) STEM images compared ultrastructure of PAO1 and PAO1ΔwspF biofilm with no treatment and following DNaseI treatment. Although the thread-like EPS largely decreased, PAO1Δ*wspF* biofilm kept structural integrity after DNaseI treatment. Red arrow highlighted unaffected thread-like eDNA at the center of clumps of vesicle-like structure and cell debris (right image). Scale bar, 1μm **(D)** STEM images of pellet sample from PAO1 biofilm showing thread-like structure outside of bacteria. Scale bar, 1μm. **(E)** STEM images of pellet sample form PAO1 biofilm following DNaseI treatment showing no apparent tread-like structure outside of PAO1 bacteria. Scale bar, 1μm. **(F)** STEM images of pellet sample of PAO1Δ*wspF* biofilm without DNaseI treatment. Scale bar, 500nm. **(G)** STEM images of PAO1Δ*wspF* biofilm after DNaseI treatment showing only trace amount of thread-like structure (red arrow) after DNaseI treatment. The inset shows the higher resolution image from the boxed area in the left images. Scale bar, 500nm.

A

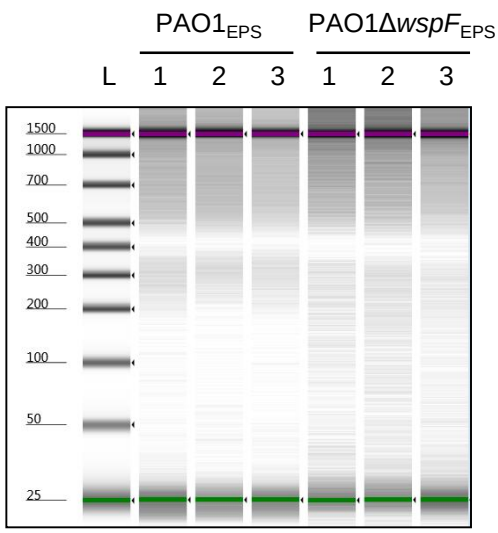

B

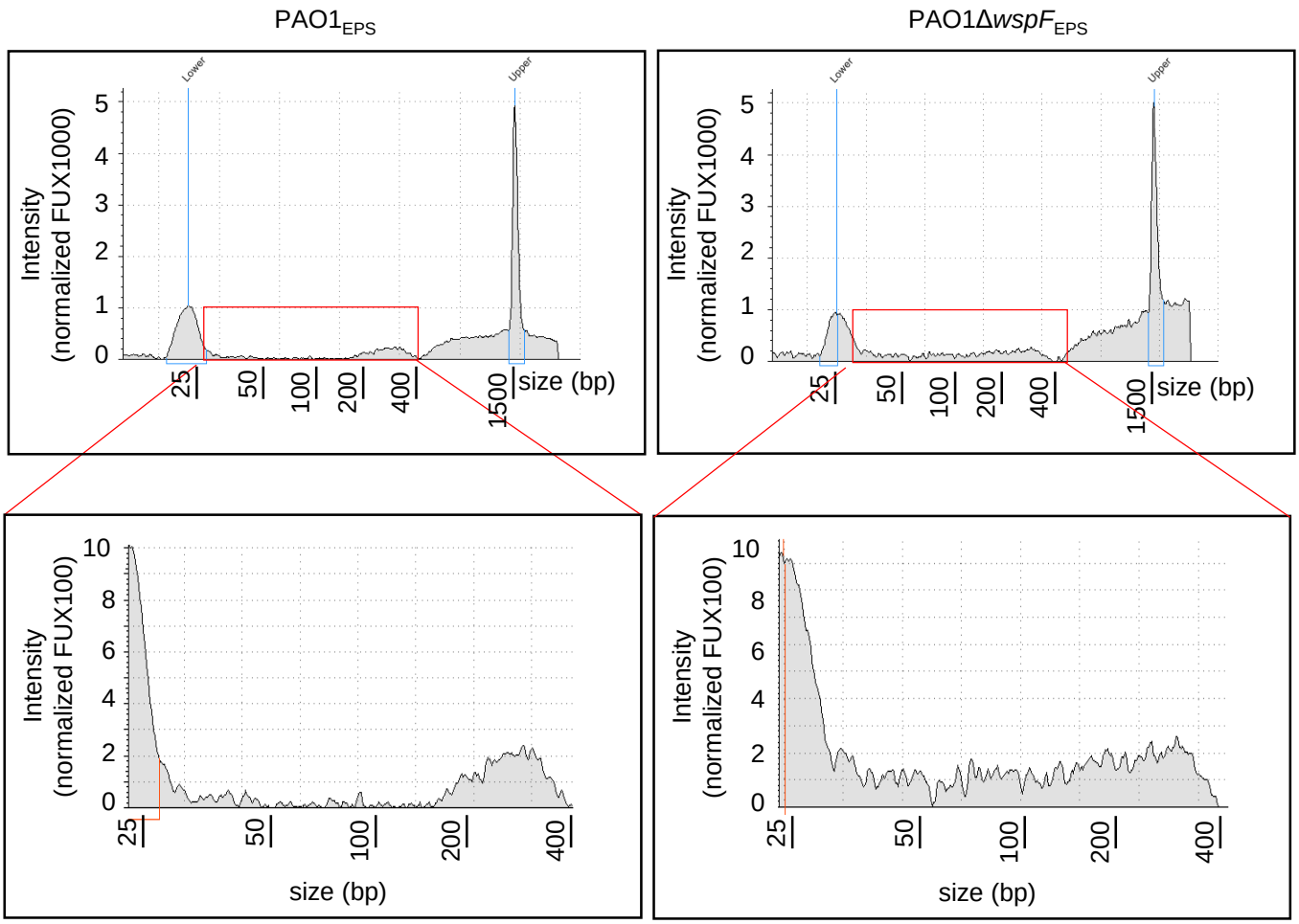

Figure S4. EPRS of eDNA from PAO1 and PAO1Δ*wspF* biofilm. Related to Figure 3. (**A**) Electron plasma resonance spectroscopy (EPRS) of the DNA isolated from the EPS of PAO1 and PAO1ΔwspF, showing higher abundance of fragmented eDNA in PAO1ΔwspF biofilm. The numerical value indicates the sample replicates. (**B**) Histogram of EPRS showing the fragmented DNA in the EPS of PAO1Δ*wspF* biofilm. The region between 400-25 bp were shown as insets.

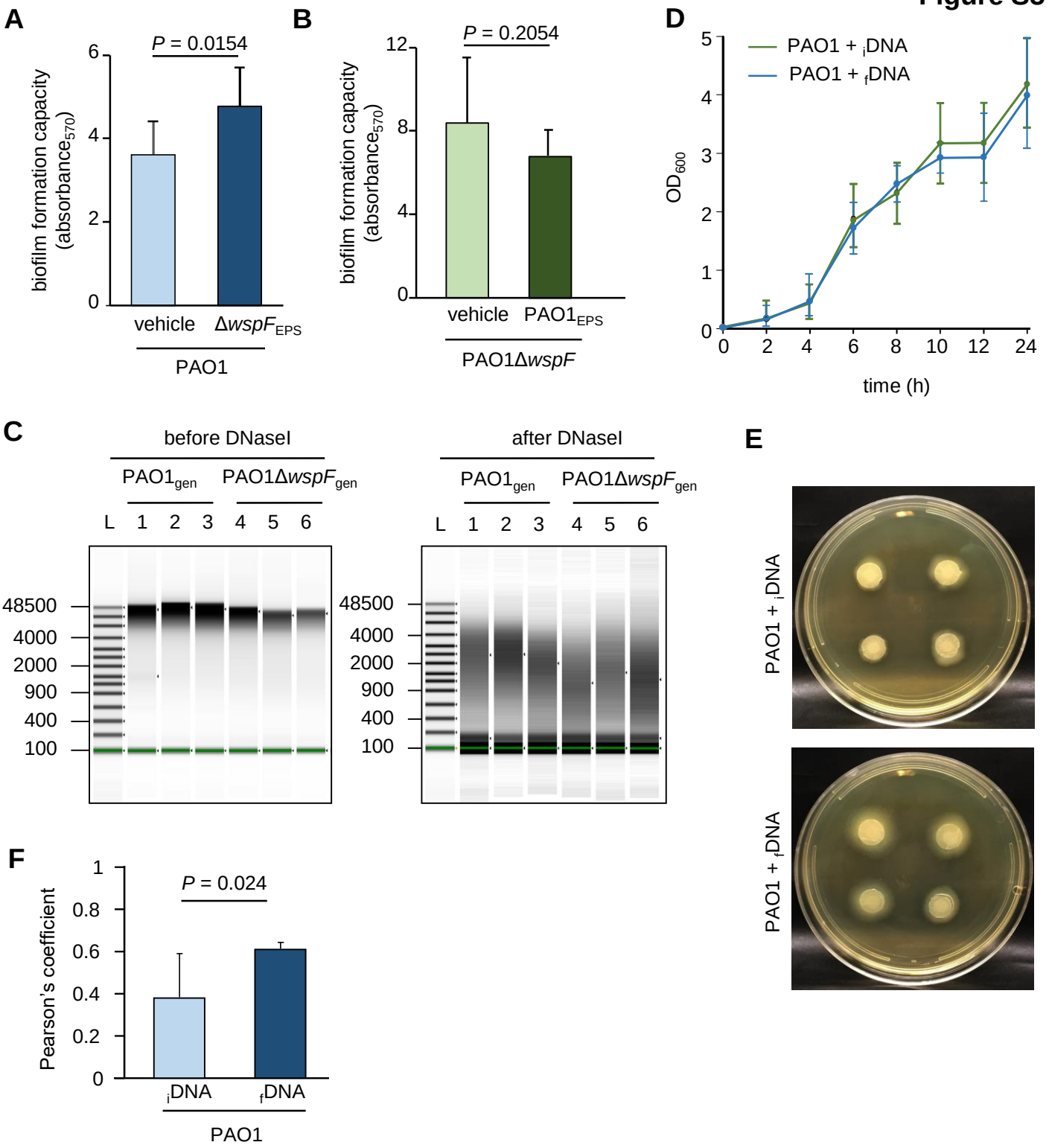

Figure S5. Effect of digested DNA on PAO1 biofilm. Related to Figure 4A-C. (A) Crystal violet assay of PAO1 hydrated biofilm at 12h treated with 1µl of PAO1*ΔwspF* EPS (2ug of eDNA). (n=8) **(B)** Crystal violet assay of PAO1*ΔwspF* hydrated biofilm at 24h treated with 1µl of PAO1 EPS (2ug of eDNA) (n=8). **(C)** Electron plasma resonance spectroscopy of the genomic DNA isolated from PAO1 and PAO1Δ*wspF*. (left panel) before DNaseI digestion and (right panel) after DNaseI digestion. **(D)** The growth curve of PAO1 after treatment with intact genomic DNA ($_i$DNA) and fragmented genomic DNA ($_f$DNA) isolated from PAO1. **(E)** The digital photomicrograph of the PAO1 biofilm at 12h treated with intact genomic DNA ($_i$DNA) and fragmented genomic DNA ($_f$DNA). (**F**) The Pearson's coefficient from fig 4B of the PAO1 biofilm at 12h treated with intact genomic DNA ($_i$DNA) and fragmented genomic DNA ($_f$DNA) were plotted graphically as mean ± SD (n=4).

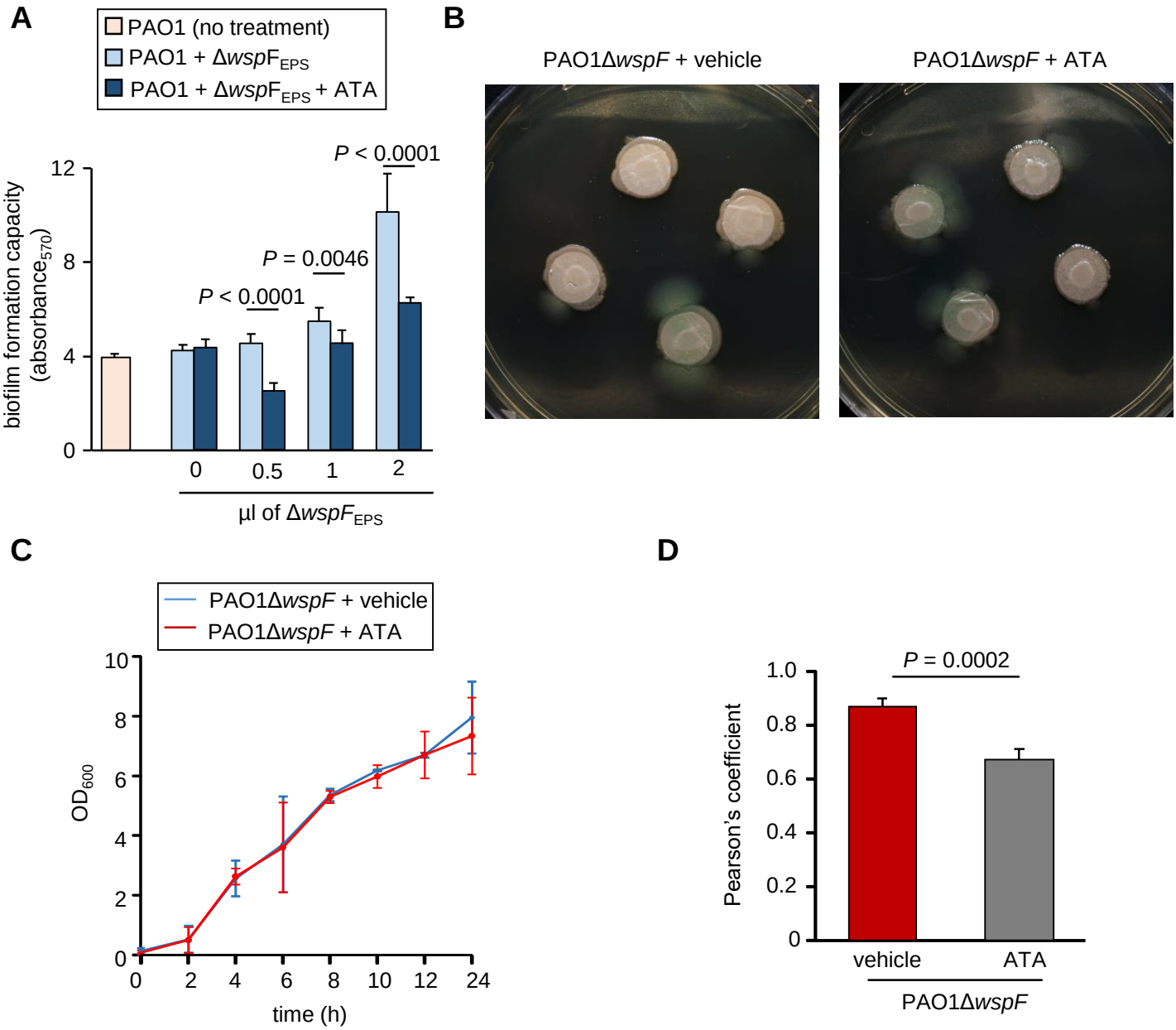

Supplementary Figure 6. Effect of ATA on PAO1Δ*wspF* biofilm. Related to Figure 4D-F. (**A**) Crystal violet assay of untreated PAO1 hydrated biofilm at 12h and PAO1 hydrated biofilm treated with different volume of PAO1Δ*wspF* EPS (1µl = 2ug of eDNA) in presence of 0.5µM of ATA (n=8). Inhibition of DNA–protein interaction compromised *in vitro* PAO1 biofilm formation. (**B**) The digital photomicrograph of the PAO1Δ*wspF* biofilm at 24h treated with buffer and ATA. (**C**) The growth curve of PAO1Δ*wspF* biofilm treated with buffer and ATA. (**D**) The Pearson's coefficient of the PAO1Δ*wspF* biofilm at 24h treated with vehicle and ATA were plotted graphically as mean ± SD (n=4).

Transparent Methods

Bacterial strain. *P. aeruginosa* prototypical strain PAO1 and its isogenic RSCV PAO1Δ*wsp*F were used in this study. Under laboratory conditions, emergence of RSCVs relies on loss-of-function mutations in the methylesterase-encoding gene *wspF* (Pu et al., 2018)**.** Cultures were routinely grown on Luria-Bertani (LB) agar or in LB broth.

***In vitro* biofilm.** *In vitro* PAO1 and PAO1Δ*wsp*F biofilm were developed on a 10 mm polycarbonate membrane (PCM) filter as described previously (Banerjee et al., 2015). Briefly, following overnight culture in LB medium at 37°C, the bacteria were inoculated on sterile PCM filters placed on trypticase soy agar (TSA) (Catalog No: 22091, Sigma-Aldrich, USA) plates. The plates were incubated at 37°C for 24h, after which the PCMs were transferred to a new TSA agar plate. The PCM filters were kept for additional 24h for the biofilm to mature.

Treatment of *in vitro* biofilm. In some experiments, the 48h matured biofilm was treated with RNase free DNaseI (Roche, 04716728001) for 30 min at 37°C prior to sample processing. The 1X buffer (Roche, 04716728001) without the DNaseI (Roche, 04716728001) was used as vehicle control. In other set of experiments, we treated the 48h biofilm cultures with 0.5µM ATA (aurintricarboxylic acid) (A1895 Sigma) for 30 min at 37°C. For PAO1 and PAO1Δ*wsp*F biofilm assays, a time point of 12h and 24h was chosen.

Bacterial growth curve. *P. aeruginosa* PAO1 and PAO1Δ*wsp*F were cultured in Luria-Burtani (LB) medium at 37°C in round bottom tubes with continuous shaking at 300 rpm. The optical density of the media at 600 nm was recorded over different time points with or without treatments and plotted graphically.

Scanning transmission electron microscopy (STEM) sample preparation. Biofilms were primarily fixed with 2.5% glutaraldehyde and 2% paraformaldehyde in 0.15M-cacodylate buffer. After washed three times with 0.15M-cacodylate buffer, the primarily fixed biofilms were post-fixed with 2% reduced osmium tetroxide. The biofilms were then washed with distilled water and further stained with 1% uranyl acetate. The stained samples were dehydrated in an increasing series of ethanol (30%, 50%, 70%, 80%, 90%, 2×100%) for 15 min each. After dehydration, samples were immersed in 1:0, 3:1, 1:1 and 1:3 acetone/resin for 60 minutes each and then kept in 100% resin overnight. Lastly the samples were transferred in fresh 100% resin and incubated at 65°C for 2 days to form a polymerized resin block.

90nm ultra-fine sections were cut from the resin block using a Reichert-Jung (Leica, Wetzlar, Germany) Ultracut E ultramicrotome. The thin sections were picked up with a loop and put on 400 meshes copper grids. For tomography, 500 nm thick sections were cut and put on copper grids with parallel bars. The thick sections were oriented so that the biofilm-growing base was perpendicular to the parallel bar. The copper grids with resin-embedded samples were air dried and then coated with 3nm thick amorphous carbon on both sides.

STEM image acquisition. Electron micrographs were collected in STEM mode on a Tecnai F20 S/TEM (Thermo Fisher Scientific, Hillsboro) with high angle angular dark field (HAADF) detector. Microscope was operated at an acceleration voltage of 200kV using Tecani Imaging and Analysis (TIA) software. Images size was 2,048×2,048 pixels. Exposure time was 25s.

STEM Tomography and data processing. STEM tomography was collected on the FEI probe-corrected Titan3™ 80-300 S/TEM (Thermo Fisher Scientific, Hillsboro). The microscope was operated at an acceleration voltage of 300kV. Images with 2,048×2,048 pixels were recorded with HAADF detector. Single-axis tilt series ranging from -65° to 65° with 1° interval steps were recorded by using the FEI Xplore3D software (Movies S7-8). Sample tilting, focusing and image shift correction were controlled by Xplore3D software. STEM dynamic focus was activated to ensure areas of interest are imaged in focus even at high tilt angles. Tracking was set after exposure. Tomographic tilt series were aligned and reconstructed using IMOD software package (University of Colorado). 3D reconstruction was built by weighted back-projection

method. Images were visualized using IMOD, Chimera and Avizo software's. Movies were made using Avizo software.

Scanning electron microscopy. Scanning electron microscopy was performed on the *in vitro* biofilm as described previously (Banerjee et al., 2015). Briefly, the biofilm on PCM filters were fixed in 4% formaldehyde / 2% glutaraldehyde solution for 48 hours at 4°C, and subsequently dehydrated in graded ethanol series. The samples were mounted on an aluminum stub and were sputter coated with gold-palladium (Au/Pd) and imaged under the scanning electron microscope (XL 30S; FEG, FEI Co., Hillsboro, OR) operating at 5 kV in the secondary electron mode.

Density gradient centrifugation of *in vitro* biofilm of PAO1 and PAO1Δ*wsp*F. 48h i*n vitro* biofilm of PAO1 and PAO1Δ*wsp*F were gently vortexed in 1 ml sterile PBS for 30s to make homogenous mixture. 20 ml Ficoll (Ficoll® Paque Plus, GE17-1440-03 SIGMA) was taken in a 50 ml centrifuge tube. The bacterial suspension was slowly poured on the Ficoll and the tube was centrifuged at 1800 g for 20 min. The supernatant and pellet were taken separately in new tubes. The supernatant was centrifuged at 12,000 g for 10 min at 4°C to collect the bacteria. Bacteria obtained from both supernatant and pellets were washed three times with sterile PBS. The bacterial pellet was then immediately processed for protein isolation. The total protein concentration was quantitated using BCA assay (Pierce, # 23228).

Fluorescence staining of biofilm and confocal microscopy: Biofilms were washed three times with sterile PBS. The density and architecture of the extracellular polymeric substances (EPS), referred to here as "extracellular matrix," was stained with 100 mg/ml FITC-conjugated Hippeastrum Hybrid Amaryllis lectins. (HHA; specific for Psl) for two hours at 4°C (Baker et al., 2015). The biofilms were then washed and fixed with 4% paraformaldehyde. Prior to imaging, the biofilms were stained with DAPI. For detection of extracellular DNA, TOTO™-1 iodide staining (ThermoFisher Scientific, Cat # T3600; dilution 1:1000) was done(Turnbull et al., 2016). Confocal microscopy was performed using Olympus FV1000 filter confocal system at 40x, N.A. 0.45 objective lens (Olympus America Inc, Melville NY). Live cell imaging was done with LSM880 laser scanning confocal microscope.

For the live dead staining of the bacteria, 48h biofilms were incubated for 30 min with a solution containing Syto Green (live) and propidium iodide (dead) (Invitrogen) as per manufacture's instruction. For the study of biofilm matrix, 48h biofilms were incubated for 45min with a solution containing Film Tracer SYPRO Ruby dye (Invitrogen) as previously described (Yi et al., 2011), with minor modifications. SYPRO Ruby fluorescence images were acquired by Olympus FV1000 filter confocal microscope with excitation at 457nm and emission at 610nm. After z-series acquisition, a z image through the image stack, perpendicular to the substrate, was generated.

Bacterial oxygen consumption assay. The XFe96 Extracellular Flux Analyzer (Seahorse Bioscience) was used to quantitate oxygen consumption rates (OCRs) as described previously. Briefly, 48h after biofilm were disrupted and separated using density gradient centrifugation. The separated fractions were diluted to an OD_{600} of ~0.3. Cells were added to XF Cell Culture Microplates pre-coated with poly-D-lysine (PDL). Cells were centrifuged for 10 min at 1,400 × g in a Multifuge ×1R (M-20 rotor) to attach them to the pre-coated plates. After centrifugation, 160µL of fresh media was added to each well.

Extracellular Polymeric Substance (EPS) isolation: EPS was isolated and purified from *in vitro* biofilm as mentioned by Bales et al. with some modifications (Bales et al., 2013). Briefly, 48h old *in vitro* biofilm was transferred into 500µL of PBS (phosphate buffered saline), and vortexed. Complete recovery of EPS was done by vortexing at least for three times. PCM membrane was discarded after recovery of EPS. 37.5% of formaldehyde was added into the cultured solution and incubated for 1 hour at room temperature on shaker (100 rpm). The treated solution was mixed with 1M sodium hydroxide and incubated for 3h at room temperature. This solution was centrifuged at 16,800g for 1 hour at 40°C. Supernatant was filtered through 0.2µm filter. EPS was stored at -80°C for further use. Sterility of purified EPS was checked by spreading 50µL of EPS on TSA agar plates followed by incubation at 37°C for 48 hours. For normalization, the total polysaccharides in EPS was measured by total carbohydrate assay kit (Sigma Aldrich, USA) following manufacture's instruction. The whole EPS was electrophoresed on 1% agarose gel for visualizing the EPS

DNA. In some experiments, the DNA was extracted from EPS using GenElute™ miniprep binding column (Sigma-Aldrich, USA) and subjected to EPRS analysis using Agilent high sensitivity D1000 tape station.

DNase assay of EPS. The DNase activity of the EPS isolated from PAO1 and PAO1Δ*wsp*F biofilm were measured using the DNaseAlert™ QC System (Invitrogen) as per manufacturer's protocol.

Crystal violet assay for biofilm quantification. *P. aeruginosa* (PAO1 and PAO1Δ*wsp*F) were cultured in Luria-Bertani (LB) medium at 37°C in pre-sterilized 96 well flat bottom polystyrene micro-titre plates in triplicates as described previously (O'Toole, 2011) with modifications. Briefly, old media was discarded, and biofilm was washed three times with PBS and air-dried. Biofilm was stained with 200 µl of crystal violet solution (Fisher Scientific, S25275B) (0.1%) and incubated at 37°C for 15 minutes. The excess crystal violet was removed from wells and washed three times with PBS. 200µl of 70% ethyl alcohol was added in each well. Plate was incubated at 37°C for 10 minutes. Biofilm growth was monitored in terms of $O.D_{570}$ nm using micro plate reader**.**

Genomic DNA isolation and agarose gel electrophoresis. Genomic DNA from PAO1 and PAO1Δ*wsp*F was isolated by GenElute™ Bacterial Genomic DNA Kit (Sigma-Aldrich, USA) following manufacturer's instructions. 1.5 mL of 10^6 CFU mL^{-1} logarithmic bacterial broth culture was taken for genomic DNA isolation. The bacterial cells were pelleted by centrifuging the tube at 12,000-16,000 g for 2 min. The pellet was resuspended in 180µL of lysis solution followed by gentle vortex. 20µL of RNase A was added to the solution and incubated for 2 min at room temperature. 20µL of proteinase K was added to the solution and incubated at 55°C for 30 min. 500µL of column preparation solution was added to each column and centrifuged at 12000 g for 1 minute. 200µL of ethanol was added to the cell lysate and mixed by vortexing for 10 s. The entire solution was transferred into the column and centrifuged at 6500 g for 1 min. The flow though was discarded, and the column was rinsed with 500µL of wash solution 1. The column was further washed with wash solution and centrifuged at 12000-16000 g for 3 min. 200µL of elution buffer was added to the column and incubated for 5 min at room temperature. Genomic DNA was eluted following centrifugation of the column at 6500 g for 1 min. Further the genomic DNA was visualized on 0.8% agarose gel and analyzed by EPRS using Agilent genomic DNA tape station.

Next Generation Sequencing: PAO1 and PAO1Δ*wsp*F EPS DNA samples were isolated and quality check was performed by Qubit DNA Assay Kit. All samples passed internal quality control. The samples were subjected to fragmentation, adaptor addition, with final QC by Agilent 2100 Bioanalyzer and real-time PCR quantification. Whole Genome Sequencing (8 Million reads, 2x75bp, PE) was performed. The reads were first trimmed for adaptor sequences and error corrected. Genome assembly was performed using SPAdes. Genomic DNA of PAO1 and PAO1Δ*wsp*F were also sequenced and compared with PAO1 reference sequence (accession number: NC_002516) showing high synteny with the reference sequence (Figure S1,2), indicating the assembly quality was adequate for subsequent analysis. Coverage analysis of each genomic region was performed. The average coverage for each EPS DNA was found to be around 300x. Read coverage was then compared between PAO1 EPS and PAO1Δ*wsp*F EPS sample. Figure 3C shows sorted alignment with PAO1 reference sequence

DNA digestion. The genomic DNA isolated from PAO1 and PAO1Δ*wsp*F strains were subjected to DNA digestion using RNase free DNaseI (Roche, 04716728001) for 30 min at 37°C. The DNA was purified to remove the DNaseI and 500 ng of either this digested DNA or intact DNA (without DNaseI treatment and purification) was added to the bacterial culture on PCM.

Statistical analysis. Samples were coded and data analysis was performed in a blinded fashion. Data were reported as mean ± SD. All experiments were performed at least three times. Student's t test (two-tailed) was used to determine significant differences. Comparisons among multiple groups were tested using analysis of variance (ANOVA). $p<0.05$ was considered statistically significant.

Supplemental References

Baker, P., Whitfield, G.B., Hill, P.J., Little, D.J., Pestrak, M.J., Robinson, H., Wozniak, D.J., and Howell, P.L. (2015). Characterization of the Pseudomonas aeruginosa Glycoside Hydrolase PslG Reveals That Its Levels Are Critical for Psl Polysaccharide Biosynthesis and Biofilm Formation. J Biol Chem *290*, 28374-28387.

Bales, P.M., Renke, E.M., May, S.L., Shen, Y., and Nelson, D.C. (2013). Purification and Characterization of Biofilm-Associated EPS Exopolysaccharides from ESKAPE Organisms and Other Pathogens. PLoS One *8*, e67950.

Banerjee, J., Ghatak, P.D., Roy, S., Khanna, S., Hemann, C., Deng, B., Das, A., Zweier, J.L., Wozniak, D., and Sen, C.K. (2015). Silver-Zinc Redox-Coupled Electroceutical Wound Dressing Disrupts Bacterial Biofilm. PLoS ONE *10*, e0119531.

O'Toole, G.A. (2011). Microtiter Dish Biofilm Formation Assay. Journal of Visualized Experiments : JoVE, 2437.

Pu, M., Sheng, L., Song, S., Gong, T., and Wood, T.K. (2018). Serine Hydroxymethyltransferase ShrA (PA2444) Controls Rugose Small-Colony Variant Formation in Pseudomonas aeruginosa. Frontiers in Microbiology *9*, 315.

Turnbull, L., Toyofuku, M., Hynen, A.L., Kurosawa, M., Pessi, G., Petty, N.K., Osvath, S.R., Cárcamo-Oyarce, G., Gloag, E.S., Shimoni, R.*, et al.* (2016). Explosive cell lysis as a mechanism for the biogenesis of bacterial membrane vesicles and biofilms. Nature communications *7*.

Yi, S., Sahni, N., Daniels, K.J., Lu, K.L., Srikantha, T., Huang, G., Garnaas, A.M., and Soll, D.R. (2011). Alternative mating type configurations (a/alpha versus a/a or alpha/alpha) of Candida albicans result in alternative biofilms regulated by different pathways. PLoS biology *9*, e1001117.